Research Network FWF S105

Photoacoustic Imaging in Medicine and Biology

http://pai.uibk.ac.at

Exact Reconstruction in Photoacoustic Tomography with Circular Integrating Detectors II: Spherical Geometry

Gerhard Zangerl and Otmar Scherzer

July 2009

PAI Report No. 17

FWF Der Wissenschaftsfonds.

universität innsbruck

Exact Reconstruction in Photoacoustic Tomography with Circular Integrating Detectors II: Spherical Geometry

Gerhard Zangerl[1] Otmar Scherzer[1,2]

[1]Department of Mathematics
University of Innsbruck
Technikerstr. 21a
6020 Innsbruck, Austria

[2]Radon Institute of Computational and Applied Mathematics
Altenberger Str. 69
4040 Linz, Austria

{Gerhard.Zangerl,Otmar.Scherzer}@uibk.ac.at

July 7, 2009

Abstract. Illuminating tissue with pulsed electromagnetic waves generates acoustic waves inside an object, which can be measured and converted into a three dimensional (3d) image. This text is concerned with a two- step reconstruction method where the acoustic pressure is measured with circular integrating detectors. In the first step reconstruction formulas for some kind of projection of the source distribution are derived in the second step an inversion formula for a circular radon transform on the sphere is developed.

Keywords: Radon transform; photoacoustic tomography; photoacoustic microscopy; Hankel transform; image reconstruction; integrating detectors.

AMS Classifications: 44A12, 65R32, 35L05, 92C55.

1 Introduction

Photoacoustic tomography (PAT), also called thermoacoustic tomography, relies on the fact that objects like tissue emit acoustic waves after a stimulation with a pulsed electromagnetic wave [10, 15, 25]. The acoustic wave generated by this pulse depends on electromagnetic absorbtion properties of the investigated object. Then it is measured outside the object and is converted into a 3d image. PAT presents a hybrid imaging technique that combines the high contrast of optical imaging with the high resolution of ultrasonic imaging.

The common approach in PAT uses small piezoelectric transducers that measure the acoustic pressure outside an object [25]. Since these transducers should mimic point like measurements reconstruction algorithms which are based on the point detector assumption yield images with a spatial resolution that is essentially limited by the size of the used piezoelectric transducers [24]. Also other limiting effects of the transducers like directivity efficiency and insensibility for certain frequencies are reported.

An approach which overcomes this limitations has been proposed in [3, 9] where either large size planar or integrating line detectors are used for data acquisition. Line shaped detectors integrate the acoustic pressure over its length and can be realized by a Mach-Zehnder or Fabry-Perot interferometer [4, 21, 20], which is an optical device that uses interference of laser beams to measure the varying acoustic pressure.

In [28] the use of so called circular integrating detectors for PAT has been proposed. Such detectors integrate the acoustic pressure over circles and detectors can be realized for instance by guiding laser beams with optical fibers [7]. The development of such detectors is motivated by mainly two practical aspects: Parts of linear integrating detectors which are distant from an object may be less influenced by the pressure wave since attenuation effects are increasing. Further, linear integrating detectors are not suitable to realize a compact experimental buildup. The use of circular integrating detectors has also been proposed independently in [27].

This paper is a sequel of [28] where the measuring circles are arranged on a cylindrical stack which encloses the object. However, this provides a compact experimental buildup only in one dimension since theoretically the cylindrical stack should have to be infinitely high. Clearly, a cylinder of finite hight cannot record acoustic waves which propagate nearly parallel to its axis and increasing its hight also has to increases the duration of the measurement process. A natural way, provided the objects of interest are small enough, is to consider circular integrating detectors which fully enclose the object. This ensures that all acoustic pressure signals emitted from the enclosed object is recorded in finite time. This improves data acquisition and reduces measurement time. It turns out that similar computations like in [28] can be reproduced if one considers circular detectors as the circles of latitude on a sphere. This will lead to exact reconstruction formulas that provide a stable inversion of the considered problem.

The outline of this article is as follows. In Section 2 the principals of PAT are reviewed and the experimental buildup for circular integrating detectors is explained. In section 3 a 2d reconstruction algorithm is derived. In section 4 stable inversion formulas are obtained and considerations on noisy data are made. The final section is concerned with the implementation of the novel and stable inversion formulas.

2 Photoacoustic Tomography with Circular Integrating Detectors

Once an object is illuminated by pulsed electromagnetic radiation it emits acoustic pressure. The pressure $p(\mathbf{x}, t)$, at time t and location $\mathbf{x} = (x, y, z) \in \mathbb{R}^3$ is recorded away from the object and is used for 3d imaging. This technique offers high contrast and resolution and has proven to be successful in medical applications including cancer diagnostics [14, 16, 23] and imaging of vasculature [12, 13, 6].

If the sound speed is spatially constant and equal to one the photoacoustic pressure field is described by the initial value problem [10, 22, 25]

$$\partial_t^2 p(\mathbf{x}, t) = \triangle p(\mathbf{x}, t)\,, \qquad (\mathbf{x}, t) \in \mathbb{R}^3 \times (0, \infty)\,, \tag{1}$$

$$p(\mathbf{x}, 0) = f(\mathbf{x})\,, \qquad \mathbf{x} \in \mathbb{R}^3\,, \tag{2}$$

$$\partial_t p(\mathbf{x}, 0) = 0\,, \qquad \mathbf{x} \in \mathbb{R}^3\,. \tag{3}$$

In mathematical terms, PAI is concerned with recovering the initial pressure $f(\mathbf{x})$ from measurements of p outside the support $\mathrm{supp}(f) = \Omega$ which is considered as a compact set in $\mathbb{R}^3$. In [28] circular integrating detectors where introduced and inversion formulas which are based on a reduction of the 3d previous wave equation in cylindrical coordinates to a 2d axial symmetric wave equation were developed. In this text similar reconstruction formulas for the case of spherical geometry are derived. This is practically reasonable since an arrangement of detectors on a sphere allows a compact buildup which makes it possible to record all the pressure emitted from an enclosed object in finite time. This buildup could be very useful for the investigation of small objects like small animals, or objects as illustrated in figure 2.

Assume $p(\mathbf{x}, t)$ is the unique solution of (1)-(3) and, for $\sigma \in S^1$, define

$$P_\sigma(r, \vartheta, t) := \frac{1}{2\pi} \int_0^{2\pi} p(\mathbf{\Phi}_\sigma(r, \vartheta, \phi), t)\, d\phi\,, \quad (r, \vartheta, t) \in \mathbb{R}_{>0} \times [0, \pi] \times \mathbb{R}_{\geq 0}\,, \tag{4}$$

$$F_\sigma(r, \vartheta) := \frac{1}{2\pi} \int_0^{2\pi} f(\mathbf{\Phi}_\sigma(r, \vartheta, \phi))\, d\phi\,, \qquad (r, \vartheta) \in \mathbb{R}_{>0} \times [0, \pi]\,, \tag{5}$$

which is the pressure and initial density integrated over the family of parallel circles

$$\mathbf{\Phi}_\sigma(r, \vartheta, \cdot) : [0, 2\pi] \to \mathbb{R}^3$$

$$\phi \mapsto D_\sigma \cdot (r \sin(\vartheta) \cos(\phi), r \sin(\vartheta) \sin(\phi), r \cos(\vartheta))\,,$$

where D_σ denotes the rotation around the $x-$axis. Finally we denote by

$$G_\sigma(\vartheta, t) := P_\sigma(r_0, \vartheta, t)\,, \qquad (\sigma, \vartheta, t) \in S^1 \times [0, \pi] \times \mathbb{R}_{\geq 0} \tag{6}$$

the measurement data. Note that the data $G_\sigma(\vartheta, \cdot)$ are supported in a finite time domain $[0, T]$ since acoustic waves in $\mathbb{R}^3$ pass every bounded region in finite time. If the sound speed is equal to one then $T = 2r_0$ is a possible choice.

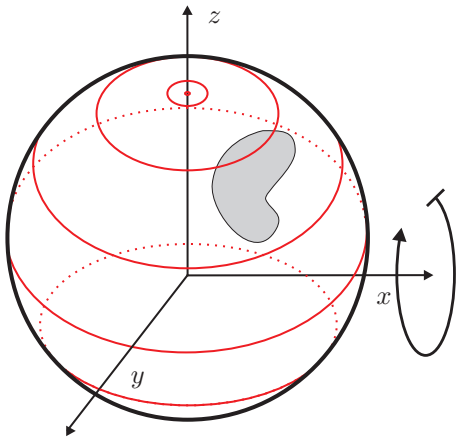

Figure 1: Scanning geometry: Circles of latitude on a sphere enclose an object and are rotated around it.

Remark 2.1. The measurement data defined in 6 are not what is directly measured by a family of parallel circles. To appreciate this suppose for a moment that the pressure is caused by a sphere in the origin. Then G_σ gives the same value for each ϑ for a fixed time t which means that the measurements are independent of the circumferences of the measuring circles. Measurement data can easily be transformed into (6) by weighting each circular measurement by its circumference.

The next section outlines an algorithm to recover the integrated initial data F_σ from the data $(G_\sigma)_{\sigma\in S^1}$.

3 Reconstruction Process

3.1 Reduction of the Wave Equation

Recovering the initial pressure from data collected with circular integrating or line detectors is based on a reduction of equations (1)-(3) to a two dimensional wave equation which finally leads to a two-stage reconstruction procedure. The same reductions holds true for the setup proposed in the previous section.

Proposition 3.1. *Let $f \in C_0^\infty(\Omega)$ and define P_σ and F_σ, $\sigma \in S^1$ by (4), (5).*

Then P_σ satisfies the wave equation

$$\partial_t^2 P_\sigma(r,\vartheta,t) = LP_\sigma(r,\vartheta,t), \qquad (r,\vartheta,t) \in \mathbb{R}_{>0}\times[0,\pi]\times\mathbb{R}_{\geq 0}\,, \tag{7}$$

$$P_\sigma(r,\vartheta,0) = F_\sigma(r,\vartheta), \qquad (r,\vartheta) \in \mathbb{R}_{>0}\times[0,\pi]\,, \tag{8}$$

$$\partial_t P_\sigma(r,\vartheta,0) = 0, \qquad (r,\vartheta) \in \mathbb{R}_{>0}\times[0,\pi]\,. \tag{9}$$

where the operator L is defined by

$$L := r^{-2}\partial_r r^2 \partial_r + r^{-2}\sin(\vartheta)^{-1}\partial_\vartheta \sin(\vartheta)\partial_\vartheta. \tag{10}$$

Proof. The proof is analogous to the one in [28] and is omitted. □

Note that the initial data of the 2d wave equation (7)-(9) for a σ is given by

$$F_\sigma(r,\vartheta) = \int_0^{2\pi} f(\Phi_\sigma(r,\vartheta,\phi))d\phi.$$

These are the integrals of f over the circles $\Phi_\sigma(r,\vartheta,\cdot)$. Reconstructiong the initial data for each σ yields the circular integrals $(F_\sigma)_{\sigma\in S^1}$. Then the function f can be reconstructed from this family of circular integrals.

3.2 Inversion Formula for the 2d Problem

In the following denote by

$$\mathbf{C}_t\left\{\phi\right\}(\omega) := \sqrt{\frac{2}{\pi}}\int_0^\infty \phi(t)\cos(\omega t)dt\,, \qquad \phi\in L^1((0,\infty))\,,\omega>0\,, \tag{11}$$

$$\mathbf{S}_t\left\{\phi\right\}(\omega) := \sqrt{\frac{2}{\pi}}\int_0^\infty \phi(t)\sin(\omega t)dt\,, \qquad \phi\in L^1((0,\infty))\,,\omega>0\,, \tag{12}$$

$$\mathbf{H}_r^l\left\{\phi\right\}(\omega) := \int_0^\infty \phi(r) j_l(\omega r)\; r^2 dr\,, \qquad \phi\in L^1((0,\infty), r^2dr)\,,\omega>0\,, \tag{13}$$

$$\phi_l := \int_0^\pi \phi(\vartheta)P_l(\cos(\vartheta))\sin(\vartheta)d\vartheta\,, \qquad \phi\in L^1((0,\pi),\sin(\vartheta)d\vartheta)\,,l\in\mathbb{N}\,, \tag{14}$$

the cosine, sine, spherical Hankel transform and the scalar product with $P_l(\cos(\vartheta))$ the $l-$th normalized Legendre polynomial, respectively. If one of the first three transformations is applied to functions depending on several variables then the transformed variable is added as subscript, e.g., $\mathbf{H}_r^l\left\{F_\sigma\right\}(\omega,\vartheta) = \int_0^\infty F_\sigma(r,\vartheta)j_l(\omega r)r^2dr$.

Theorem 3.1. *Let $F_\sigma(r,\vartheta)$ and $G_\sigma(r,t)$ be given by (5), (6). Then F_σ is related to the measurement data G_σ by the formula*

$$\mathbf{H}_r^l\left\{F_{\sigma,l}\right\}(\omega) = \sqrt{\frac{2}{\pi}}\,\frac{\mathbf{C}_t\left\{G_\sigma\right\}_l(\omega)}{\omega^2 j_l(r_0\omega)}. \tag{15}$$

Proof. The separation Ansatz $R(r)S(\vartheta)\cos(\omega t)$ to equation to (7) and performing some manipulations, yields the ode's

$$\cot(\vartheta)\partial_\vartheta S + \partial_\vartheta^2 S + l(l+1)S = 0, \quad \frac{r^2}{R}\left[\frac{2}{r}\partial_r R + \partial_r^2 R\right] + r^2\omega^2 - l(l+1) = 0. \tag{16}$$

It is well known that the first equation is solved by the legendre polynomials $P_l(\cos(\vartheta))$ whereas the solutions of the second equation are given by the spherical bessel functions $j_l(rw)$. Thus for all $l \in \mathbb{N}$ the function

$$(r, \vartheta, t) \mapsto \omega^2 j_l(r\omega) P_l(\cos(\vartheta))\cos(\omega t)$$

is a bounded solution of (7) and (9). A general solution of equations (7)-(9) can formally be written as superposition

$$P_\sigma(r, \vartheta, t) = \sum_{l=0}^{\infty} \int_0^\infty \bar{F}_{\sigma,l}(\omega)\, \omega^2 j_l(r\omega) P_l(\cos(\vartheta))\cos(\omega t) d\omega, \tag{17}$$

where it is assumed that the Legendre Polynomials are already normalized, i.e. $\| P_l \|_2 = 1$. Evaluating this expression at $t = 0$ yields

$$F_\sigma(r, \vartheta) = \sum_{l=0}^{\infty} \int_0^\infty \bar{F}_{\sigma,l}(\omega)\omega^2 j_l(r\omega) P_l(\cos(\vartheta)) d\omega.$$

Therefore its scalar product with the $l-$th Legendre Polynomial is given by

$$F_{\sigma,l}(r) = \int_0^\infty \bar{F}_{\sigma,l}(\omega)\, \omega^2 j_l(r\omega) d\omega.$$

Thus $\bar{F}_{\sigma,l}(\omega) = \mathbf{H}_r^l \{F_{\sigma,l}\}(\omega)$ and after substituting $r = r_0$ in (17) one has $P_\sigma(r_0, \vartheta, t) = G_\sigma(\vartheta, t)$ and therefore

$$\mathbf{C}_t \{G_\sigma\}(\vartheta, \omega) = \sqrt{\frac{\pi}{2}} \sum_{l=0}^{\infty} \mathbf{H}_r^l \{F_{\sigma,l}\}(\omega)\, \omega^2 j_l(r_0\omega)\, P_l(\cos(\vartheta)). \tag{18}$$

Using the orthogonality relation for Legendre polynomials implies

$$\mathbf{C}_t \{G_\sigma\}_l(\omega) = (\pi/2)^{1/2}\, \mathbf{H}_r^l \{F_{\sigma,l}\}(\omega)\, \omega^2 j_l(r_0\omega), \tag{19}$$

and thus (15) follows. □

It is interesting to note that this formula has got the same structure like Norton's famous inversion formula [18] which has been applied to photoacoustic tomography, e.g., in [1, 8].

3.3 Solving the 2nd Problem: Factorization Method

Once the inverse problem for the 2d problem (7)-(9) is solved for each σ, the second reconstruction step is concerned with the determination of f from its integrals $F_\sigma(r,\vartheta)$ over the family of circles $c_{r\vartheta\sigma} := \Phi_\sigma(r,\vartheta,\cdot)$, where $(r,\vartheta,\sigma) \in [0,r_0] \times [0,\pi]^2$. Consider a sphere S_ρ of fixed radius $r = \rho$ centered at the origin O and pick out those circles from the family which are lying on S_ρ. The circular means of $f|_{S_\rho}$, the restriction of f on S_ρ, over this circles are then given by $F_\sigma(\rho,\vartheta)$. Further, note that this family of circles is arranged along a great circle on S_ρ so that their *spherical midpoints* lie on it. Then this family of circles can be related to the average of a function over circles centered on a line via stereographic projection like shown in figure 2.

To state the results some notation is introduced:

- Let C_ρ denote the great circle on S_ρ which is contained in the yz plane and is parameterized by $\varphi_\rho(\sigma) = (0, \rho\cos(\sigma), \rho\sin(\sigma))$.
- Let $\mathbf{p} = (0,0,\rho) \in C_\rho$ and $z^\perp$ be the xy plane and denote by

$$\pi_\rho : S_\rho \setminus \{\mathbf{p}\} \to z^\perp,\ \mathbf{x} \mapsto \left(\frac{x}{\rho - z}, \frac{y}{\rho - z}\right) \tag{20}$$

  the stereographic projection from S_ρ onto $z^\perp$.
- Let $\mathcal{C}_0^\infty(S_\rho)$ be the space of infinitely differentiable functions with all derivatives vanishing at the north pole $\mathbf{p}$ and define the circular mean transform on S_ρ

$$(R_\rho h)(\vartheta,\sigma) := \int_0^{2\pi} h(\Phi_\sigma(\rho,\vartheta,\phi))d\phi \tag{21}$$

  over the circle $c_{\rho\vartheta\sigma}$ for any $h \in \mathcal{C}_0^\infty(S_\rho)$.
- Finally for every function $g \in \mathcal{C}^\infty(\mathbb{R}^2)$ let the integral

$$\mathbf{F}_{xy}\{g\}(\xi,\eta) := \int_{\mathbb{R}^2} g(x,y)e^{-i(x\xi+y\eta)}dxdy, \tag{22}$$

  provided it exists, denote its Fourier transform.

Remark 3.1. Since the stereographic projection π_ρ is a conformal map the image $\pi_\rho(c_{\rho\vartheta\sigma}) := C_{yt}$ of any circle is a circle again. Further the computation

$$(R_\rho f|_{S_\rho})(\vartheta,\sigma) = \int_{c_{\rho\vartheta\sigma}} f(\mathbf{x})dc_{\rho\vartheta\sigma}(\mathbf{x}) = \tag{23}$$

$$\int_{C_{yt}} (f|_{S_\rho} \circ \pi_\rho^{-1})(x,y)\frac{2dC_{yt}(x,y)}{1+x^2+y^2} \tag{24}$$

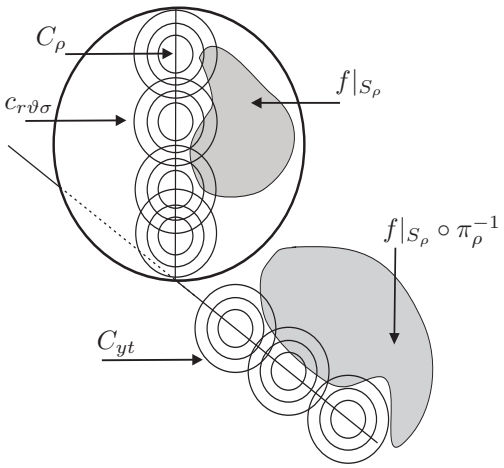

Figure 2: Circles of latitude arranged on a great circle on S_ρ After Stereographic projection one obtains the means over circles centered on a line.

holds. If there is an inversion formula for the circular means over the family of circles $\pi_\rho\left(c_{\rho\vartheta\sigma}\right)$ in the plane one is able to reconstruct the function

$$g(x,y) := \frac{2}{1+x^2+y^2}\ (f|_{S_\rho} \circ \pi_\rho^{-1})(x,y) \tag{25}$$

and thus one is able to compute the desired function $f|_{S_\rho}(\pi_\rho^{-1}(x,y))$.

Lemma 3.1. *Consider a circle C_{yt} in the xy plane with midpoint $(0,y)$ on the y axis and radius t. Then $\pi_\rho^{-1}(C_{yt}) = c_{\rho\vartheta\sigma}$ is the circle with*

$$\sigma(y,t) = \frac{1}{2}\arctan\left(\frac{2y\rho}{y^2-t^2-\rho^2}\right),\ \vartheta(y,t) = \frac{1}{2}\arctan\left(\frac{2t\rho}{y^2-t^2+\rho^2}\right). \tag{26}$$

Proof. The antipodal points $(y\pm t,0)$ of a circle C_{yt} are mapped onto those points on S_ρ by π_ρ^{-1} which have the spherical coordinates $(\rho,\sigma^\pm,0) = (\rho, 2\arctan(\rho/(y\pm t),0)$. The spherical midpoint of $c_{\rho\vartheta\sigma}$ has got the coordinates $(\rho,\sigma(y,t),0)$ with $\sigma(y,t) = (\sigma^+ + \sigma^-)/2$. Further its radius, the arclength on S_ρ from its midpoint to its boundary, is given as $\vartheta(y,t) = (\sigma^- - \sigma^+)/2$. The circle on S_ρ with this midpoint and radius is just given by $\Phi_\sigma(\rho,\vartheta,\cdot) = c_{\rho\vartheta\sigma}$. The simplified expressions for $\vartheta(y,t)$ and $\sigma(y,t)$ are given in (26). □

Theorem 3.2 (Factorization method)**.** *Let $\rho > 0$, $f|_{S_\rho} \in \mathcal{C}_0^\infty(S_\rho)$ be symmetric with respect to the yz plane and g be like in (25). Then g can be reconstructed by*

$$\mathbf{F}_{xy}\left\{g\right\}(\xi,\eta) = \pi\,|\eta|\ \mathbf{F}_{yt}\left\{Rg\right\}\left(\sqrt{\xi^2+\eta^2},\eta\right), \tag{27}$$

where $Rg(y,t)$ is given by formula (28).

Proof. Let C_{yt} be any circle in $z^\perp$ like in the previous lemma and g be the function (25). Then its circular mean over C_{yt} is given by

$$(Rg)(y,t) = \int_{C_{yt}} g(t\cos(\alpha), y + t\sin(\alpha))d\alpha \tag{28}$$

According to the previous lemma and the remark the values of these integrals are given by $(R_\rho f)(\vartheta(y,t), \sigma(y,t))$ for all y and t. Further note that the function g is symmetric with respect to the y axis since f is symmetric with respect to the yz plane and due to [11] from $f \in \mathcal{C}_0^\infty(S_\rho)$ it follows that g is a rapidly decreasing function on $\mathbb{R}^2$. The reconstruction of such functions from their means over circles with midpoints on a line is well treated for instance in [2]. The fourier inversion formula which is stated in the theorem is derived in there. □

Remark 3.2. Although the reconstruction method above requires that $f|_{S_\rho}$ is symmetric in practice it is sufficient if it is supported in only one of the half spheres separated by the yz plane. Then one can always interpret the values of the integrals $F_\sigma(\rho, \vartheta)$ as integrals over a symmetric object.

4 Stable Formulas for Wave Inversion

A direct implementation of formula (15) will cause serious numerical problems since the denominator becomes zero for certain values of ω. Similar to [8, 28] this problem will be circumvented by expanding F_σ into a spherical bessel series and employing (15).

In the following let (ω_{nl}) for $l \in \mathbb{N}$ denote the zeros of the function $\omega \mapsto j_l(r_0\omega)$.

Theorem 4.1. *The function F_σ from (8) is reconstructed from the measuremnt data (6) by the formula*

$$F_\sigma(r,\vartheta) = \sqrt{\frac{2}{\pi}} \sum_{l\in\mathbb{N}} \sum_{n\in\mathbb{N}} \frac{\mathbf{S}_t \left\{tG_\sigma\right\}_l (\omega_{nl}) j_l(r\omega_{nl})}{\omega_{nl}^2 j_{l+1}(r_0\omega_{nl})^3} P_l(\cos(\vartheta)). \tag{29}$$

Proof. Since $f \in \mathcal{C}_0^\infty(\Omega)$ the functions $F_{\sigma,l}(\cdot)$ are supported in $[0, r_0]$ and thus can be expanded into a series of spherical bessel functions

$$F_{\sigma,l}(r) = \sum_{n\in\mathbb{N}} \mathbf{H}_r^l \left\{F_{\sigma,l}\right\} (\omega_{nl}) \frac{j_l(r\omega_{nl})}{j_{l+1}(r_0\omega_{nl})^2}. \tag{30}$$

For exact measurement data the enumerator in (15) has to be zero whenever the denominator is zero. Thus one can use the rule of D'Hospital to evaluate $\mathbf{H}_r^l \left\{F_{\sigma,l}\right\}$ at ω_{nl}:

$$\begin{aligned}(\pi/2)^{1/2} \mathbf{H}_r^l \left\{F_{\sigma,l}\right\} (\omega_n) &= \lim_{\omega\to\omega_{nl}} \frac{\partial_\omega \mathbf{C}_t \left\{G_\sigma\right\}_l (\omega)}{\partial_\omega\, \omega^2 j_l(r_0\omega)} \\ &= \lim_{\omega\to\omega_{nl}} \frac{-\mathbf{S}_t \left\{tG_\sigma\right\}_l (\omega)}{2\omega j_l(r_0\omega) + w^2\, \partial_\omega j_l(r_0\omega)} = \frac{\mathbf{S}_t \left\{tG_\sigma\right\}_l (\omega_{nl})}{\omega_{nl}^2 j_{l+1}(r_0\omega_{nl})},\end{aligned}$$

where the last expressions follow from the identities $\partial_\omega j_l(\omega) = \frac{l}{\omega} j_l(\omega) - j_{l+1}(\omega)$ and $\partial_\omega \mathbf{C}_t\{tG_\sigma\} = -\mathbf{S}_t\{tG_\sigma\}$. □

The expansion into a series of spherical bessel functions in formula (29) can be implemented stable and can also be used to derive a second inversion formula. The following result can easily be obtained from the expansion formulas in derived in [26].

Proposition 4.1. *Let f_σ^m and g_σ^m denote the fourier coefficients of the functions $f(\mathbf{\Phi}_\sigma(z,r,\phi))$ and $g_\sigma(\vartheta,\phi,t) := p(\mathbf{\Phi}_\sigma(r_0,\vartheta,\phi),t)$, where f and p are the unique solution of (1)-(3), with respect to ϕ. Then*

$$\mathbf{H}_r^l\{f_{\sigma,l}^m\}(\omega) = \frac{2}{\pi}\frac{\mathbf{F}_t\{g_{\sigma,l}^m\}(\omega)}{\omega^2\, h_l^{(1)}(r_0\omega)}, \qquad \omega\in\mathbb{R},\ l\in\mathbb{N}, \tag{31}$$

with $h_l^{(1)}$ denoting the l-th order Hankel function of the first kind.

Due to $F_{\sigma,l} = f_{\sigma,l}^0$ and $G_{\sigma,l} = g_{\sigma,l}^0$ and the fact that in the denominator of (31) this proposition leads immediately to a second inversion formula, given in the following

Theorem 4.2. *With the same assumptions as in theorem 4.1*

$$F_\sigma(r,\vartheta) = \frac{2}{\pi}\sum_{l\in N}\sum_{n\in\mathbb{N}} \frac{\mathbf{F}_t\{G_{\sigma,l}\}(\omega_{nl})}{\omega_{nl}^2\, h_l^{(1)}(r_0\omega_{nl})}\frac{j_l(rv_n)P_l(\cos(\vartheta))}{j_{l+1}(r_0\omega_{nl})^2}. \tag{32}$$

Proof. □

Remark 4.1. In Xu and Wang [26] they use the source term formulation

$$\begin{aligned} \Delta p(\mathbf{x},t) - \partial_t^2 p(\mathbf{x},t) &= f(\mathbf{x})\frac{d\delta(t)}{dt} \\ p(\mathbf{x},t) = \partial_t p(\mathbf{x},t) &= 0,\ \ t<0 \end{aligned}$$

of the wave equation which for is equivalent to the initial value problem (1)-(3) for $t>0$. Then their derivation of (31) is based on a series expansion of a Green function, which arises in an integral representation for the temporal Fourier transform of p [17]:

$$\frac{e^{i\omega(|\Phi_\sigma(r_0,\vartheta,\phi)-\Phi_\sigma(r,\vartheta,\phi)|)}}{|\Phi_\sigma(r_0,\vartheta,\phi)-\Phi_\sigma(r,\vartheta,\phi)|} = \sum_{l=0}^{\infty} j_l(\omega r)h_l^{(1)}(\omega r_0)P_l(\cos(\vartheta)). \tag{33}$$

Then (31) is derived straight forward using orthogonality relations for the Legendre polynomials and bessel functions.

4.1 Noisy Data

In practise only noisy measurement data, write $G^\delta := G^\delta_\sigma$, are available and generically there is no solution of system (7)-(9) such that $P(r_0, \vartheta, t) = G^\delta(\vartheta, t)$. In other words this means that $G^\delta \notin \mathrm{ran(A)}$ where A is the operator which maps a function F onto $P\,|_{\{r=r_0\}}$ where P is the solution of (7)-(9). However, it turns out that formula (29) makes sense for noisy data G^δ which are contained in a bigger space than ran(A).

In the following let

$$L^2 := L^2([0,\pi] \times [0,T], \sin(\vartheta) d\vartheta, dt)$$

the space of square integrable functions.

Theorem 4.3. *Formulas (29), (32) define continuous operators from $L^2 \to L^2$.*

Proof. The assertion in the theorem 4.3 is proven here for formula (29) only since the proof for (32) is almost analogous. Note that for any $G^\delta \in L^2$ the function $\omega \mapsto \mathbf{S}_t \left\{ tG^\delta \right\}(\omega)$ is continuous and thus it makes sense to evaluate it at the discrete points ω_{nl}. Since the legendre polynomials P_l form an orthonormal basis in $L^2([0,\pi], \sin(\vartheta)d\vartheta)$ the coefficients G^δ_l defined by (14) are in l^2. On the other hand note that the functions $t \mapsto \sin(2kt\pi/T)$ are orthogonal in $L^2(0,T)$ and that ω_{nl} approaches infinity like $l + cn$ for any $c > 0$. Thus for any k choose ω_{nl} to be as close to $2k\pi/T$ as possible from above and write $2k\pi/T + \epsilon = \omega_{nl}$. Then, using the addition formulas, it immediately follows

$$\left| \mathbf{S}_t \left\{ tG^\delta \right\}(\omega_{nl}) \right| = \left| \int_0^T tG^\delta(t) \sin((2k\pi/T + \epsilon)t) dt \right| \leq$$

$$\left| \int_0^T tG^\delta(t) \sin(2kt\pi/T) dt \right| + \left| \int_0^T tG^\delta(t) \cos(2kt\pi/T) dt \right|,$$

which means that $|\, \mathbf{S}_t \left\{ tG^\delta \right\}(\omega_{nl})|$ is bounded by the the sum of the absolue values of its fourier coefficients with respect to $\{\sin(2k\pi/T), \cos(2k\pi/T)\}$. Therefore $\mathbf{S}_t \left\{ tG^\delta \right\}_l (\omega_{nl})$ lies in l^2 for varying l and n. The remaining term in series expansion (29), except the basis functions $P_l(\cos(\vartheta))$, $j_l(r\omega_{nl})/j_{l+1}(r_0\omega_{nl})$ and $\mathbf{S}_t \left\{ tG^\delta \right\}_l (\omega_{nl})$ is $1/(\omega^2_{nl} j^2_{l+1}(\omega_{nl}))$. Since

$$j_l(r_0\omega) = \cos\left(r_0\omega - \frac{(l+1)\pi}{2} - \frac{\pi}{4} \right) \frac{1}{r_0\omega} + O\left(\frac{1}{\omega} \right)$$

the latter term is bounded and therefore the series (29) converges for any $G^\delta \in L^2$. □

This result ensures that for each of the reconstruction formulas above there is a constant M such that

$$\| F - F^\delta \|_2 \leq M \| G - G^\delta \|_2 < M\delta.$$

This guarantees that the reconstruction error becomes small if the measurements are accurate enough.

The theorem guarantees that formulas (29) and (32) are valid for measurement data in L^2. A bybroduct of this result is that one can deduce new series identies for the characteristic function. Since the derivation is essentially the same for both formulas the result is presented here for formula (32) only. In the following the abbreviation $\omega_n := \omega_{n0}$ is used.

Corollary 4.1. The characteristic function on $[0, a]$ can be expanded as

$$\chi_{[0,a]}(r) = \sum_{n\in\mathbb{N}} \left[e^{-i\omega(r_0-a)} \left(1 - ia\omega\right) - e^{-i\omega(r_0+a)} \left(ia\omega + 1\right) \right] \frac{j_0(r\omega_n)}{2r_0\omega_n^3 j_1(r_0\omega_n)^3}, \quad (34)$$

where the equality has to be understood in the L^2 sense.

Proof. Consider the pressure emitted by a characteristic sphere centered at the origin of radius a

$$p(\mathbf{x}, t) = \frac{r-t}{2r} \chi_{[0,a]} \left(|r-t|\right), \; \| \mathbf{x} \| = r.$$

In this special case the measurement data are given by $G(t, \vartheta) = P(r_0, \vartheta, t)$. Since there is no dependence on the angular variable ϑ in formula (29) it is summed over n only. Computation of the integral

$$\mathbf{F}_t \left\{G\right\}(\omega) = \int_{r_0-a}^{r_0+a} \frac{r_0 - t}{2r_0} e^{-i\omega t} dt$$

and inserting in (32) gives (34). □

Also the sequence $\chi_{[0,a]}/a$ tends to the dirac measure δ in the distributional sense when $a \to 0$. Thus one can also, using de L'hospital, have a new series expansion formula for the dirac measure given by

$$\delta(r) = \frac{2}{i} \sum_{n\in\mathbb{N}} e^{-i\omega_n r_0} \frac{1 + \omega_n^2}{\omega_n^3} \frac{j_0(r\omega_n)}{j_1(r_0\omega_n)^3} \quad (35)$$

5 Numerical Experiments

In practice only discrete measurement data

$$\mathtt{G}_\mathtt{s}[\mathtt{m}, \mathtt{n}] := G_{\sigma_1}(\vartheta_\mathtt{m}, t_\mathtt{n}), \qquad (\mathtt{s}, \mathtt{m}, \mathtt{n}) \in \{1, \ldots \mathtt{N}_\sigma\} \times \{1, \ldots \mathtt{N}_\vartheta\} \times \{1, \ldots \mathtt{N}_t\},$$

are available. Here $\sigma_\mathtt{s} = \pi(\mathtt{s}-1)/\mathtt{N}_\sigma$, $\vartheta_\mathtt{m} = \pi(\mathtt{m}-1)/\mathtt{N}_\vartheta$ and $t_\mathtt{n} = 2r_0(\mathtt{n}-1)/\mathtt{N}_t$ are discrete samples of the variables for which a measurement is performed. The aim is to find an approximation for the integrated initial pressure (5)

$$\mathrm{F}_\mathtt{s}[\mathtt{m}, \mathtt{n}] = F_{\sigma_\mathtt{s}}(r_\mathtt{n}, \vartheta_\mathtt{m}), \qquad (\mathtt{s}, \mathtt{m}, \mathtt{n}) \in \{1, \ldots \mathtt{N}_\sigma\} \times \{1, \ldots \mathtt{N}_\vartheta\} \times \{1, \ldots \mathtt{N}_r\},$$

where $r_{\mathtt{n}} = r_0(\mathtt{n}-1)/\mathtt{N}_r$ and $\mathtt{N}_r = \mathtt{N}_t/2$. After such an approximation is calculated one can reconstruct a discrete approximation to f by applying the fourier inversion formula of [2] for a fixed fixed $\mathtt{n}$.

First a discretization of formula (14) applied to the measurement data is given by

$$\mathtt{G_s}[\mathtt{l},\mathtt{n}] := \sum_{\mathtt{m}=1}^{\mathtt{N}_\vartheta} \mathtt{G_s}[\mathtt{m},\mathtt{n}]\ P_{\mathtt{l}}(\cos(\vartheta_{\mathtt{m}}))\sin(\vartheta_{\mathtt{m}}),\ l \in \{0,\dots,\mathtt{N}_\vartheta\} \tag{36}$$

where the P_l are the normalized Legendre polynomials. The discrete sine transform, applied to the second component of the measurement data multiplied by t evaluated at ω_{nl} is implemented by

$$\mathtt{S}_t\left\{t\mathtt{G_s}\right\}[\mathtt{l},\mathtt{j}] := \left(\frac{2}{\pi}\right)^{1/2} \sum_{\mathtt{n}=1}^{\mathtt{N}_t} t_{\mathtt{n}}\mathtt{G_s}[\mathtt{l},\mathtt{n}]\ \sin\!\left(t_{\mathtt{n}}\omega_{\mathtt{l}\mathtt{j}}\right), \qquad \mathtt{j} \in \{0,\dots,\mathtt{N}_r-1\}\,. \tag{37}$$

The Fourier transform with respect to the time variable is as usually implemented by

$$\mathbf{F}_t\left\{\mathtt{G_s}\right\}[\mathtt{l},\mathtt{j}] = \left(\frac{1}{2\pi}\right)^{1/2} \sum_{\mathtt{n}=0}^{\mathtt{N}_t} \mathtt{G_s}[\mathtt{l},\mathtt{n}]\, e^{it_{\mathtt{n}}\omega_{\mathtt{l}\mathtt{j}}},\ \mathtt{j} \in \{0,\dots,\mathtt{N}_t-1\} \tag{38}$$

and evaluated with the FFT algorithm. This finally leads to the discrete versions of inversion formula (29)

$$\mathtt{F_s}[\mathtt{n},\mathtt{m}] := \sqrt{\frac{2}{\pi}} \sum_{\mathtt{l}=0}^{\mathtt{N}_\vartheta} \sum_{\mathtt{j}=0}^{\mathtt{N}_r-1} \frac{\mathtt{S}_t\left\{t\mathtt{G_s}\right\}[\mathtt{l},\mathtt{j}]}{\omega_{\mathtt{j}\mathtt{l}}^2} \frac{j_{\mathtt{l}}(r_{\mathtt{n}}\omega_{\mathtt{j}\mathtt{l}})P_{\mathtt{l}}(\cos(\vartheta_{\mathtt{m}}))}{j_{\mathtt{l}+1}(r_0\omega_{\mathtt{j}\mathtt{l}})^3} \tag{39}$$

and (32)

$$\mathtt{F_s}[\mathtt{n},\mathtt{m}] := \frac{2}{\pi} \sum_{\mathtt{l}=0}^{\mathtt{N}_\vartheta} \sum_{\mathtt{j}=0}^{\mathtt{N}_r-1} \frac{\mathtt{F}_t\left\{\mathtt{G_s}\right\}[\mathtt{l},\mathtt{j}]}{\omega_{\mathtt{j}\mathtt{l}}^2\, h_{\mathtt{l}}^{(1)}(r_0\omega_{\mathtt{j}\mathtt{l}})} \frac{j_{\mathtt{l}}(r_{\mathtt{n}}\omega_{\mathtt{j}\mathtt{l}})P_{\mathtt{l}}(\cos(\vartheta_{\mathtt{m}}))}{j_{\mathtt{l}+1}(r_0 v_{\mathtt{j}})^2}. \tag{40}$$

A short discussion of the computational complexity of the previous implementation should be considered. For simplicity assume that the same number of samples, i.e. $\mathtt{N}_\vartheta = \mathtt{N}_r = \mathtt{N}_t = \mathtt{N}_\sigma =: \mathtt{N}$, for each variable is taken and that the values of the sine the spherical Bessel function and those of the Legendre polynomials are pre-computed and stored in lookup tables. Then the evaluation (38) needs $\mathcal{O}(\mathtt{N}^2\log\mathtt{N})$ floating point operations (FLOPS) whereas (37), (36), (29) and (32) require $\mathcal{O}(\mathtt{N}^3)$ FLOPS. Applying the inversion formula (27) also requires $\mathcal{O}(\mathtt{N}^3)$ FLOPS. For three dimensional imaging (38), (37),(36), (29), (or inversion formula (32)) and the filtered back-projection formula have to be applied $\mathtt{N}$ times. Thus the total number of FLOPS is estimated as

$$\mathtt{N}_{\mathrm{FLOPS}} = \mathtt{N}\left(\mathcal{O}(\mathtt{N}^2\log\mathtt{N}) + \mathcal{O}(\mathtt{N}^3) + \mathcal{O}(\mathtt{N}^3) + \mathcal{O}(\mathtt{N}^3)\right) = \mathcal{O}(\mathtt{N}^4)\,. \tag{41}$$

Note that $3d$ back-projection type formulas based on point like measurement data have complexity $\mathcal{O}(\mathtt{N}^5)$.

Numerical experiments for the values $\mathrm{R} = 1$ and $T = 2$ are performed. The synthetic initial data f is assumed to be a superposition of radially symmetric objects around centers $\mathbf{x}_n$, i.e.,

$$f(\mathbf{x}) = \sum_n f_n\big(\|\mathbf{x} - \mathbf{x}_n\|\big)\,, \qquad \mathbf{x} \in \mathbb{R}^3\,.$$

The acoustic pressure generated by a single radially symmetric object at position $\mathbf{x}$ and time t is given by (see [10])

$$p_n(\mathbf{x}, t) = \frac{\|\mathbf{x} - \mathbf{x}_n\| - t}{2\,\|\mathbf{x} - \mathbf{x}_n\|}\, f_n\Big(\big|\,\|\mathbf{x} - \mathbf{x}_n\| - t\big|\Big). \tag{42}$$

By the superposition principle the total pressure is

$$p(\mathbf{x}, t) = \sum_{n=1}^{N} p_n(\mathbf{x}, t)\,, \qquad (\mathbf{x}, t) \in \mathbb{R}^3 \times (0, \infty)\,.$$

The measurement data $G_\sigma(z,t) = 1/(2\pi)\int_0^{2\pi} p(\Phi_\sigma(r_0, \vartheta, \phi), t)d\phi$, see (4), (6), were generated by evaluating of (42) followed by a numerical integration over ϕ.

Figure 3 shows a vertical cross section of the initial pressure f and the measurement data G_σ where Gaussian noise with a variance of 10% of the maximal data value is added.

The reconstructions of F_σ with (39) from exact and noisy data are depicted in Figure 5 from formula (39) and with formula (40) in Figure (6). Note that the reconstructed images do not have blurred boundaries . Moreover the images reconstructed with (29) are less sensitive to noise.

6 Conclusion

In this article a novel experimental buildup for PAT using circular integrating detectors was proposed. For collecting measurement data a fiber based Fabry-Perot interferometer can be used as an circular integrating detector. It is shown that the 3D imaging problem is reduced to a series of 2D problems. This decomposition can be used to reduce the operation count of derived reconstruction algorithms. Stable exact reconstruction formulas for the case that the object is contained in in a sphere with circles of latitude as detecting circles.

Acknowledgement

This work has been supported by the Austrian Science Foundation (FWF) within the framework of the NFN "Photoacoustic Imaging in Biology and Medicine", Project S10505-N20.

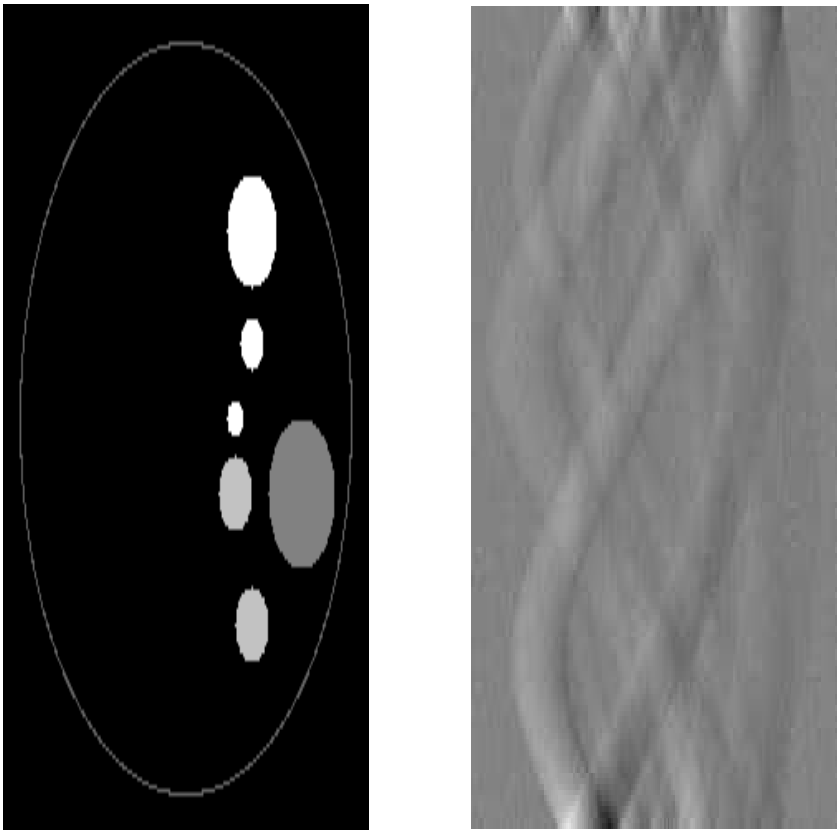

Figure 3: Left: Cross section of an ensemble of 6 absorbing spheres (x versus z). Right: The measurement data with 10% Gaussian noise added (ϑ versus t).

References

[1] G. Ambartsoumian and P. Kuchment. A range description for the planar circular Radon transform. *SIAM J. Math. Anal.*, 38(2):681–692, 2006.

[2] L. E. Andersson. On the determination of a function from spherical averages. *SIAM J. Math. Anal.*, 19(1):214–232, 1988.

[3] P. Burgholzer, C. Hofer, G. Paltauf, M. Haltmeier, and O. Scherzer. Thermoacoustic tomography with integrating area and line detectors. *IEEE Trans. Ultrason., Ferroeletr., Freq. Control*, 52(9):1577–1583, 2005.

[4] P. Burgholzer, C. Hofer, G. Paltauf, G. J. Matt, M. Haltmeier, and O. Scherzer. Thermoacoustic tomography using a fiber based Fabry–Perot interferometer as an integrating line detector. In *[19]*, 2006.

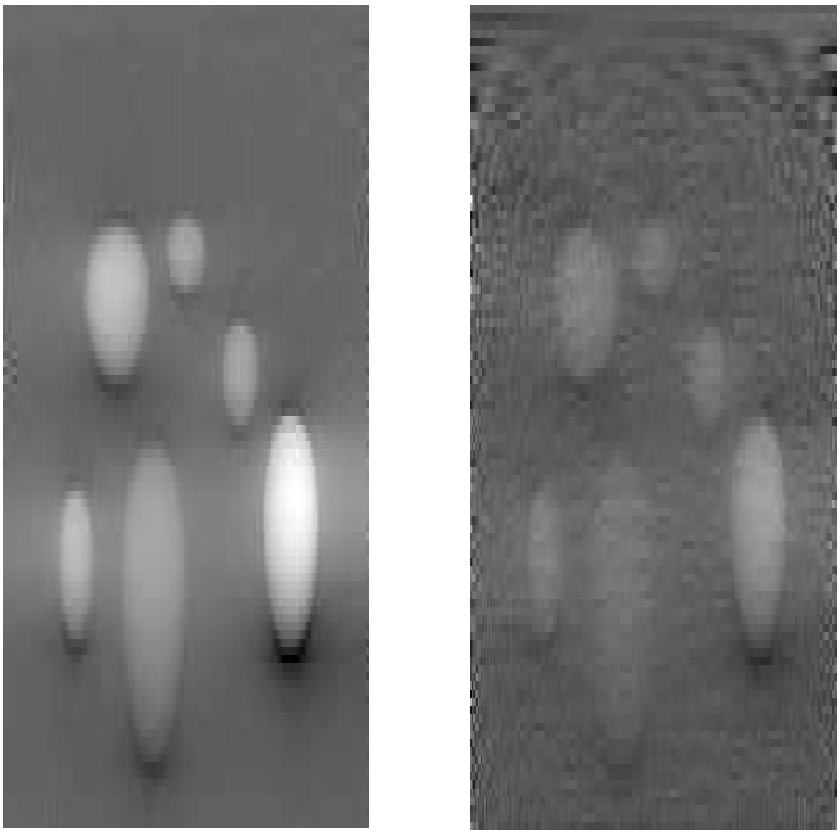

Figure 4: Reconstruction from simulated (left) and noisy data (right) with formula (39).

[5] C. Depeursinge, editor. *Novel Optical Instrumentation for Biomedical Applications III*, volume 6631 of *Proceedings of SPIE-OSA*, 2007.

[6] R. O. Esenaliev, I. V. Larina, K. V. Larin, D. J. Deyo, M. Motamedi, and D. S. Prough. Optoacoustic technique for noninvasive monitoring of blood oxygenation: a feasibility study. *App. Opt.*, 41(22):4722–4731, 2002.

[7] H. Grün, M. Haltmeier, G. Paltauf, and P. Burgholzer. Photoacoustic tomography using a fiber based Fabry–Perot interferometer as an integrating line detector and image reconstruction by model-based time reversal method. In *[5]*, 2007.

[8] M. Haltmeier, O. Scherzer, P. Burgholzer, R. Nuster, and G. Paltauf. Thermoacoustic tomography & the circular Radon transform: Exact inversion formula. *Math. Models Methods Appl. Sci.*, 17(4):635–655, 2007.

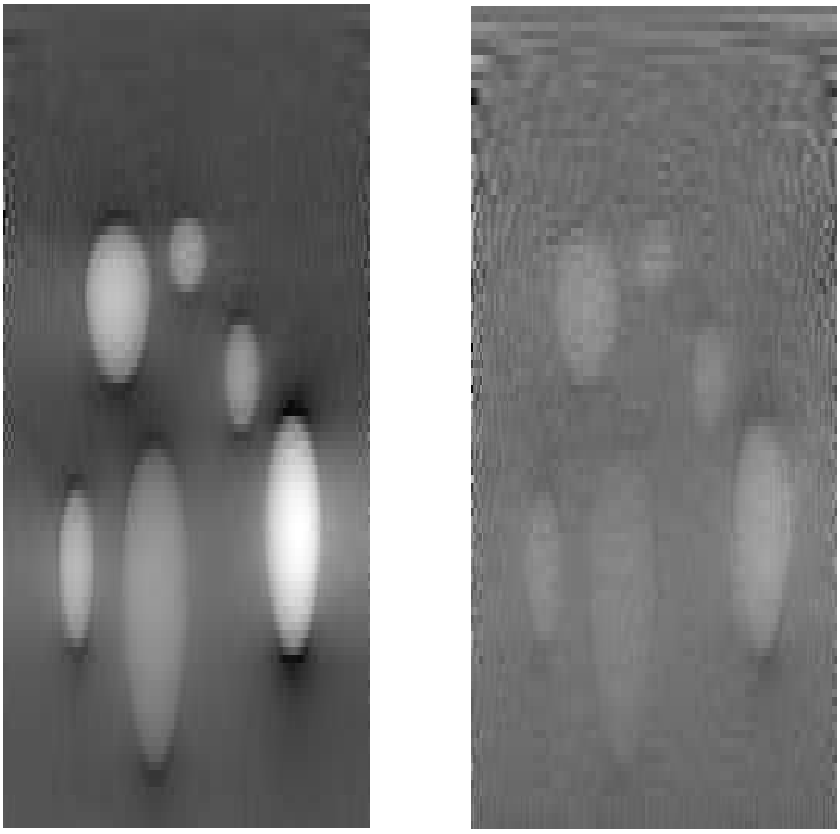

Figure 5: Reconstruction from simulated (left) and noisy data (right) (40).

[9] M. Haltmeier, O. Scherzer, P. Burgholzer, and G. Paltauf. Thermoacoustic imaging with large planar receivers. *Inverse Probl.*, 20(5):1663–1673, 2004.

[10] M. Haltmeier, T. Schuster, and O. Scherzer. Filtered backprojection for thermoacoustic computed tomography in spherical geometry. *Math. Methods Appl. Sci.*, 28(16):1919–1937, 2005.

[11] S. Helgason. *The Radon Transform*, volume 5 of *Progress in Mathematics*. Birkhäuser, Boston, second edition, 1999.

[12] C. G. A. Hoelen, F. F. M. de Mul, R. Pongers, and A. Dekker. Three-dimensional photoacoustic imaging of blood vessels in tissue. *Opt. Letters*, 23(8):648–650, 1998.

[13] R. G. M. Kolkman, E. Hondebrink, W. Steenbergen, and F. F. M. De Mul. In vivo photoacoustic imaging of blood vessels using an extreme-narrow

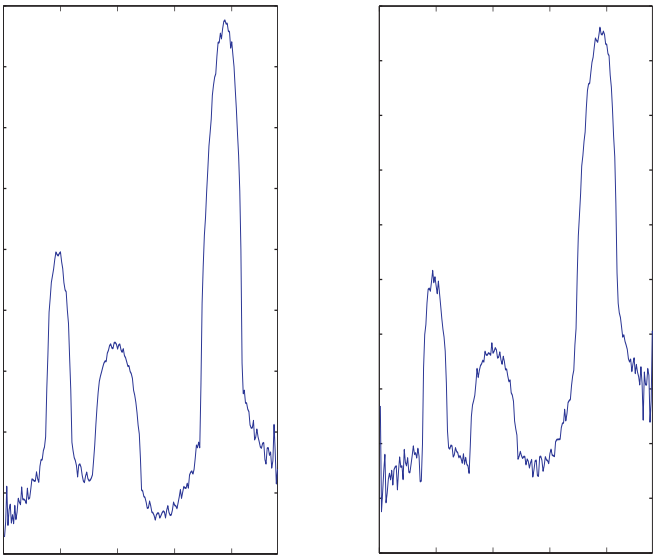

Figure 6: Cross section through the lower three spheres in the reconstructed images from simulated data. Left from formula (29) and right from formula (32).

aperture sensor. *IEEE J. Sel. Topics Quantum Electron.*, 9(2):343–346, 2003.

[14] R. A. Kruger, K. D. Miller, H. E. Reynolds, W. L. Kiser, D. R. Reinecke, and G. A. Kruger. Breast cancer in vivo: contrast enhancement with thermoacoustic CT at 434 MHz-feasibility study. *Radiology*, 216(1):279–283, 2000.

[15] P. Kuchment and L. A. Kunyansky. Mathematics of thermoacoustic and photoacoustic tomography. *European J. Appl. Math.*, 19:191–224, 2008.

[16] S. Manohar, A. Kharine, J. C. G. van Hespen, W. Steenbergen, and T. G. van Leeuwen. The Twente Photoacoustic Mammoscope: system overview and performance. *Physics in Medicine and Biology*, 50(11):2543–2557, 2005.

[17] P.M. Morse and H. Feshbach. *Methods of Theoretical Physics*. McGraw-Hill Book Co., New York, 1953. 2 volumes.

[18] S. J. Norton. Reconstruction of a two-dimensional reflecting medium over a circular domain: Exact solution. *J. Acoust. Soc. Amer.*, 67(4):1266–1273, 1980.

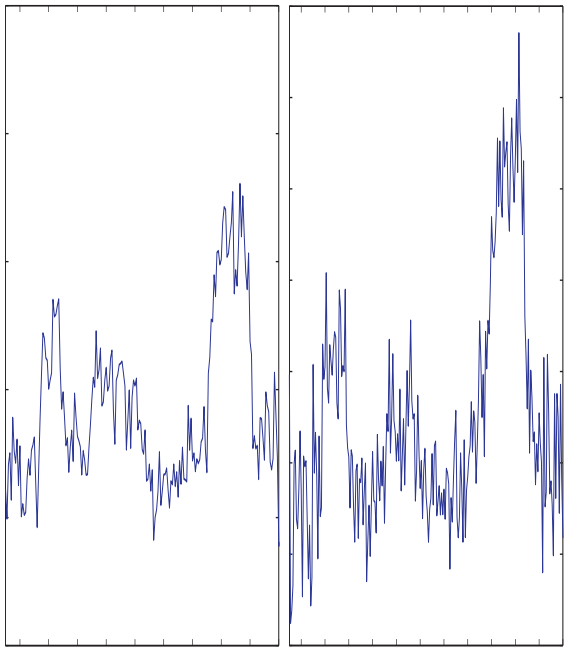

Figure 7: Cross section through the lower three spheres in the reconstructed images from noisy data. Left from formula (29) and right from formula (32).

[19] A. Oraevsky and L. V. Wang, editors. *Photons Plus Ultrasound: Imaging and Sensing 2006: The Seventh Conference on Biomedical Thermoacoustics, Optoacoustics, and Acousto-optics*, volume 6086 of *Proceedings of SPIE*, 2006.

[20] G. Paltauf, R. Nuster, M. Haltmeier, and P. Burgholzer. Experimental evaluation of reconstruction algorithms for limited view photoacoustic tomography with line detectors. *Inverse Probl.*, 23(6):81–94, 2007.

[21] G. Paltauf, R. Nuster, M. Haltmeier, and P. Burgholzer. Thermoacoustic computed tomography using a mach-zehnder interferometer as acoustic line detector. *App. Opt.*, 46:3352–3358, 2007.

[22] O. Scherzer, M. Grasmair, H. Grossauer, M. Haltmeier, and F. Lenzen. *Variational Methods in Imaging*, volume 167 of *Applied Mathematical Sciences*. Springer, New York, 2009.

[23] X. D. Wang, Y. Xu, M. Xu, S. Yokoo, E. S. Fry, and L. V. Wang. Photoacoustic tomography of biological tissues with high cross-section resolution: Reconstruction and experiment. *Med. Phys.*, 29(12):2799–2805, 2002.

[24] M. Xu and L. V. Wang. Analytic explanation of spatial resolution related to bandwidth and detector aperture size in thermoacoustic or photoacoustic reconstruction. *Phys. Rev. E*, 67(5):0566051–05660515 (electronic), 2003.

[25] M. Xu and L. V. Wang. Photoacoustic imaging in biomedicine. *Rev. Sci. Instruments*, 77(4):1–22, 2006. Article ID 041101.

[26] Minghua Xu and Lihong V. Wang. Time-domain reconstruction for thermoacoustic tomography in a spherical geometry. *Med. Phys.*, 21(7):814–822, 2002.

[27] X. Yang and L. V. Wang. Ring-based ultrasonic virtual point detector with applications to photoacoustic tomography. *Applies Physics Letters*, 90(25):251103, 2007.

[28] G. Zangerl, M. Haltmeier, and O. Scherzer. Circular integrating detectors in photo and thermoacoustic tomography. *Inverse Probl. Sci. Eng.*, 17(1):133–142, 2009.